



Soil organo-mineral associations formed by co-precipitation of Fe, Si and Al in presence of organic ligands

Wuhib Zewde Tamrat, Jérôme Rose, O. Grauby, Emmanuel Doelsch, Clément Levard, Perrine Chaurand, Isabelle Basile-Doelsch

► To cite this version:

Wuhib Zewde Tamrat, Jérôme Rose, O. Grauby, Emmanuel Doelsch, Clément Levard, et al.. Soil organo-mineral associations formed by co-precipitation of Fe, Si and Al in presence of organic ligands. *Geochimica et Cosmochimica Acta*, 2019, 260, pp.15-28. <10.1016/j.gca.2019.05.043>. <hal-02272705>

HAL Id: hal-02272705

<https://amu.hal.science/hal-02272705v1>

Submitted on 29 Aug 2019

HAL is a multi-disciplinary open access archive for the deposit and dissemination of scientific research documents, whether they are published or not. The documents may come from teaching and research institutions in France or abroad, or from public or private research centers.

L'archive ouverte pluridisciplinaire **HAL**, est destinée au dépôt et à la diffusion de documents scientifiques de niveau recherche, publiés ou non, émanant des établissements d'enseignement et de recherche français ou étrangers, des laboratoires publics ou privés.



Copyright - All rights reserved

Soil organo-mineral associations formed by co-precipitation of Fe, Si and Al in presence of organic ligands

TAMRAT Wuhib Zewde¹, Jérôme ROSE¹, Olivier GRAUBY², Emmanuel DOELSCH³, Clément LEVARD¹, Perrine CHAURAND¹, Isabelle BASILE-DOELSCH^{1*§}

1- Aix Marseille Univ, CNRS, IRD, INRA, Coll France, CEREGE, Aix-en-Provence, France

2- Aix-Marseille Univ – UMR 7325 CINaM/CNRS, campus de Luminy, 13288 Marseille Cedex 9, France

3- CIRAD, UPR Recyclage et risque, F-34398 Montpellier, France

*Corresponding author: basile@cerege.fr

Abstract

Weathering of silicates supplies a range of cations (mainly Si, Al, Fe, but also Ca, Mg, Na, K, Mn) to the soil solution. There, cations can interact with charged functional groups of dissolved soil organic matter (OM). Unlike Al and Fe, Si does not directly bind to natural OM. However, the role of Si in the mechanisms of OM stabilization by coprecipitation with short range order mineral phases (SRO) may have been underestimated. The formation of coprecipitates was tested by titrating a biotite-weathering solution up to pH 5 in presence of 3,4-Dihydroxy-L-phenylalanine (DOPA) with initial (Fe+Al):C ratio ranging from 3 to 0.003. Size, crystallinity, chemical composition and the local structure of the coprecipitates were analyzed by TEM-EDX and Fe K-edge EXAFS. Coprecipitates are amorphous particles whatever the (Fe+Al):C ratio, but their size, composition and local structure were nevertheless seen to progressively vary with increasing C content. In low C samples (high (Fe+Al):C), coprecipitates were 2-40 nm in size and were dominated by Si (30 to 70%). Fe represented only 20-50% of the mineral phase and was structured in small oligomers of Fe octahedra. Around 20% of the Fe of the coprecipitates were bound to C. Conversely, in high C samples (low (Fe+Al):C), coprecipitates were 10-90 nm in size and Fe was the main component (45-70%). Fe was almost exclusively linked to OM by monomeric Fe-O-C bonds. Si (5-40%) and Al (15-35%) were able to form oligomers occluded in the Fe-OM network. In samples with intermediate C content ((Fe+Al):C=0.3), the coprecipitates had 5-200 nm size particles. We suggest these coprecipitates are structured in a loose irregular 3D network of amorphous small oligomers of Fe (25-75%), Si (15-50%), and Al (10-35%), forming an amorphous and open-structured mineral skeleton. Within this mineral network, we suggest the organic compounds are linked either by bonds with Fe and Al to the skeleton, by monomeric Fe-O-C in the porosity of the network, or by weak bonds with other OM. This conceptual model provides an alternative to the standard view that SRO-OM is formed by ferrihydrite and amorphous Al(OH)₃. We suggest naming the structure “Nanosized Coprecipitates of inorganic oligomers with organics” with

§ Present address: CSIRO, Gate 4, Waite Road, Urrbrae SA 5064, Australia

40 “nanoCLICs” as acronym. The presence of Si in the inorganic structures may have an impact
41 not only on the amount of OM stabilized by the nanoCLICs, but in the longer term, on the
42 persistence of the OM stabilization potential by metallic oligomers.
43
44

1 Introduction

Organo-mineral interactions are known to play a key role in stabilizing organic matter (OM) in soils (Baldock and Skjemstad, 2000; Kleber et al., 2015; Kögel-Knabner et al., 2008; Schmidt et al., 2011), because bonds between organic compounds and mineral surfaces minimize microbial degradation of organic compounds (Eusterhues et al., 2014; Jones and Edwards, 1998; Porras et al., 2018; Saidy et al., 2015; Scheel et al., 2007b). Understanding the mechanisms governing the formation of organo-mineral associations is therefore a major challenge in view of increasing soil C stocks (Minasny et al., 2017; Paustian et al., 2016). Colloidal and short-range-order (SRO) minerals are increasingly considered as important mineral phases in the control of OM dynamics (Basile-Doelsch et al., 2005; Basile-Doelsch et al., 2007; Basile-Doelsch et al., 2015; Bonnard et al., 2012; Finley et al., 2018; Keiluweit et al., 2015; Kramer and Chadwick, 2018; Levard et al., 2012; Rasmussen et al., 2018). Indeed, their very small size (ranging from a few nanometers to a few tens of nanometers) and their poorly crystallized structure provide them with both large surface reactivity and large specific surfaces. These properties mean SRO is highly capable of binding with some functional groups of soil OM.

The Fe and Al oxy-hydroxides interacting with OM have been mainly studied using experimental batch approaches with either natural OM extracts or low molecular weight organic compounds (for a review, see Kleber et al. (2015)). Two formation processes have been investigated: adsorption (reaction of OM to post-synthesis SRO) and co-precipitation (formation of SRO in the presence of OM). Studies that compared the two processes showed that coprecipitation resulted in much higher maximum C contents than adsorption (Chen et al., 2014; Mikutta et al., 2014; Mikutta et al., 2011). According to Mikutta et al. (2011), coprecipitation is a process wherein monomeric or polymeric aqueous metal species (Al or Fe) form a mixed metal-organic solid from the solution after reacting with organic compounds. To experimentally address the question of how Fe and Al interact with OM at the molecular level in the coprecipitates, spectroscopic and scattering probes are required (Chen et al., 2016), and extended X-ray absorption fine structure (EXAFS) spectroscopy is one of the most useful methods to study local Fe coordination environments at molecular scale (Chen et al., 2014; Karlsson and Persson, 2010; Karlsson et al., 2008; Mikutta, 2011; Rose et al., 1998; Vilg   et al., 1999b). EXAFS makes it possible to refine the speciation of Fe by distinguishing (1) SROs (polymers made of a few dozen atoms organized at the scale of a few nanometers), (2) oligomers (i.e. dimers of 2 atoms, trimers of 3 atoms or a slightly larger number of non-ordered atoms), and (3) monomers (a single atom). Soil scientists often use SRO to refer to these different forms of Fe, as opposed to the Fe of well-crystallized oxides. To be more rigorous, we use the terms Fe-nanophase (without OM) and Fe-coprecipitate (with OM) when the speciation of Fe is not given. By extension, we use Al-nanophase and Al-coprecipitate in the same way.

In the case of Fe-coprecipitates, SRO_{Fe}-OM are often described as spherical 2-5 nm ferrihydrite crystallites aggregated in an OM matrix (Chen et al., 2016; Eusterhues et al., 2008; Mikutta et al., 2008; Mikutta et al., 2014; Schwertmann et al., 2005). This model of Fe oxy-hydroxide occlusion in OM is well illustrated in several studies (Du et al., 2018; Eusterhues et al., 2014; Kleber et al., 2015). The density of SRO_{Fe}-OM aggregates (Eusterhues et al., 2008; Guenet et al., 2017; Mikutta, 2011; Mikutta et al., 2008) together with the size of the ferrihydrite crystallites and their crystallinity (Eusterhues et al., 2008; Mikutta, 2011; Mikutta et al., 2010;

Schwertmann et al., 2005) has been shown to vary with the experimental conditions. In a limited number of studies, Fe-coprecipitates were reported to be formed by Fe-oligomers, without reaching the polymerization level of ferrihydrite (Angelico et al., 2014; Mikutta, 2011; Vilg  et al., 1999b). Other authors frequently reported that a variable proportion of mononuclear Fe formed Fe-OM complexes (Chen et al., 2016; Eusterhues et al., 2008; Karlsson and Persson, 2010, 2012; Karlsson et al., 2008; Mikutta et al., 2010; Schwertmann et al., 2005). Thus, as a function of the Fe:C ratio (from 100 down to 0.01, Kleber et al. (2015)), OM composition and pH, several Fe phases may coexist: (1) polymerized nano-oxy-hydroxides (dominant at high Fe:C ratios); (2) oligomeric clusters (dominant at intermediate Fe:C ratios); and (3) mononuclear complexes (dominant at low Fe:C ratios) (Chen et al., 2016; Mikutta, 2011). These co-existing phases led Guenet et al. (2017) to propose a model of fractal organization of Fe-coprecipitates. Aside from the differences in the structure of Fe-coprecipitates described in the studies cited above, all the authors acknowledge that the strong complexation between Fe and OM hinders the polymerization of Fe by occupying the crystal growth sites. Using low molecular weight organic compounds made it possible to focus on the main organic ligands involved in the Fe-O-C bindings. For example, Mikutta (2011) showed that catecholate bonds are more efficient in complexing Fe than carboxylate and salicylate bonds, and also that the position of the phenol group on an aromatic ring rather than the number of phenol groups controls the ligand's interaction with Fe.

Concerning Al, despite the fact that aqueous cationic Al concentration in oxic soil pore water may exceed that of Fe (because Al is more soluble than Fe hydroxides (Scheel et al., 2007b)), Al-coprecipitates have received less attention than Fe-coprecipitates with respect to the problem of OM in the soil. This may be because X ray spectroscopic techniques are much more difficult to implement for Al than for Fe. Nevertheless, like Fe, the Al phases in coprecipitates are described as solid amorphous phases (often noted $\text{Al}(\text{OH})_3$) as well as monomeric Al, both interacting with OM in proportions that vary with the experimental conditions (Mikutta et al., 2011; Scheel et al., 2007b; Schneider et al., 2010). The local structure of the polymerized Al phases has rarely been described, except when nuclear magnetic resonance approaches were used, when it was shown that OM may hinder the polymerization of tridecamer (Al_{13}), limiting the speciation of Al to small oligomers (dimers and trimers) and monomers (Masion and Bertsch, 1997; Masion et al., 2000). Thus, like for Fe, the extent of polymerization of Al in Al-coprecipitates varies with Al:C ratio, pH and nature of OM.

However, soil solutions are not pure Al or Fe solutions. A limited number of studies focused on the formation of multi-cation coprecipitates. By testing mixtures of Al and Fe, Mikutta et al. (2014) observed low amounts of Al in the Fe-Al-coprecipitates, and that the presence of Al did not affect ferrihydrite crystallinity. Nierop et al. (2002) also concluded that Fe binds more readily to OM than does Al, but noted that the initial metal/carbon ratio (M:C, M being Fe+Al) also controlled the Fe:Al ratio in the Fe-Al-coprecipitates (Vilg  et al., 1999a).

Although silicon is one of the main elements in soils, it has rarely been considered as an element of interest in batch synthesis of coprecipitates. This is due to the non-charged form of Si (neutral $\text{Si}(\text{OH})_4$ at the pH of soil solutions), which shows that Si does not spontaneously link with natural OM (Pokrovski and Schott, 1998). However, the presence of Si may modify the structures of the Fe-coprecipitates and Al-coprecipitates. In natural systems, imogolite type materials are also examples of Si bearing $\text{SRO}_{\text{Al,Si}}$ known to stabilize large amounts of OM

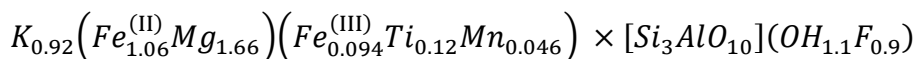
in andosols (Basile-Doelsch et al., 2005; Basile-Doelsch et al., 2007; Levard et al., 2012). Finally, in systems containing no OM, it has been shown that Si inhibits Fe polymerization, the local structure of Fe-Si-nanophases varying with the Si:Fe ratio, pH, and redox state (Doelsch et al., 2000, 2002; Doelsch et al., 2001). Recently, the formation of SRO was also tested in a more complex solution including Fe, Al, Si, Mg, K obtained through experimental biotite weathering (Tamrat et al., 2018). These authors showed that the nanophases were amorphous particles 10–60 nm in size, whose composition (dominated by Fe and Si) was strongly controlled by pH. At pH 4.2 and pH 7, the structure of the nanophases was dominated by Fe oligomers. Its polymerization was hindered by Al, Si, Mg and K. At pH 5, the Fe-Fe coordination number was even lower, polymerization being counteracted by the precipitation of high amounts of Si.

The present work is based on three hypotheses: (1) Fe-coprecipitate and Al-coprecipitate systems are not the only coprecipitates to take into account in OM stabilization issues; (2) In soils in which silicate minerals are present and provide a range of cations upon weathering, not only $\text{Fe}(\text{OH})^{2+}$ and $\text{Al}(\text{OH})^{2+}$ but also $\text{Si}(\text{OH})_4$, Mg^{2+} , Ca^{2+} , K^{2+} , etc. contribute to the structures of the coprecipitates; (3) Si, which does not directly interact with OM, also contributes to the formation of metal-OM-coprecipitates in soils. To verify these hypothesis, we tested the capacity of dissolved Fe Al and Si to form Fe-Al-Si-coprecipitates in presence of an organic ligand. Coprecipitates were formed in batch experiments by titrating a biotite-weathered solution up to pH 5 (Tamrat et al., 2018) in presence of OM. 3,4-Dihydroxy-L-phenylalanine (DOPA) was selected as a model of OM for three reasons: (1) it is a low molecular weight organic compound and low molecular weight organic compounds are known to be the main OM compounds stabilized (Lehmann and Kleber, 2015; Sutton and Sposito, 2005), (2) using a single molecule avoids uncertainties linked to fractionation of natural OM during coprecipitation (Eusterhues et al., 2011; Mikutta et al., 2007; Scheel et al., 2007b; Schneider et al., 2010) and (3) functional groups of DOPA (amine, carboxyl, aromatic ring and hydroxyl groups) represent main functional groups known in organo-mineral stabilization processes (Mikutta, 2011; Zimmerman et al., 2004). Coprecipitation at pH 5 was preferred to emphasize the effects of Si (Tamrat et al., 2018) while the molar M:C ratios ranged between 3 and 0.003. Together with the Fe-Al-Si-nanophases synthesized without OM (Tamrat et al., 2018), this series covers the range of experimental M:C conditions used in previous Fe- and Al-coprecipitate studies (Kleber et al., 2015). The present work focused on the characterization of size, crystallinity and chemical composition of Fe-Al-Si-coprecipitates by TEM-EDX and of their local structure using Fe k-edge EXAFS (extended X-ray absorption fine structure) spectroscopy. The main objectives of the paper are (1) to describe the structure of Fe-Al-Si-coprecipitates at the local scale as a function of the M:C ratio; (2) to propose a conceptual model of the coprecipitates' structure in a Fe, Al, Si and OM system; (3) to evaluate the potential implications of the presence of such Fe-Al-Si-coprecipitates in soils with respect to the concepts of organomineral interactions.

2 Materials and Methods

2.1 Materials

The weathered biotite came from Bancroft, Ontario Canada (Ward Science) and had the following chemical composition:



3,4-Dihydroxy-L-phenylalanine $[(HO)_2C_6H_3CH_2CH(NH_2)CO_2H]$ (Sigma Aldrich) was used (Figure A1) as a model of a soil organic compound. It presents the following functional groups: amine, carboxyl and an aromatic ring with double hydroxyl groups. At pH5, the amine group exists in NH_3^+ state, carboxyl group in COO^- and phenol groups in OH state. The main expected interactions with cations are carboxylate binding (Chen et al., 2016), phenol binding (Chen et al., 2016) and catecholate binding, through both OH carried by adjacent C in the aromatic ring (Mikutta, 2011). The nine C in this compound accounted for nine C atoms in subsequent molar metal to carbon ratios (M:C).

2.2 Synthesis of the coprecipitates

The coprecipitates were synthesized in two steps. The first step consisted of leaching in an acidic batch solution to collect the leachate solution containing dissolved species induced by biotite weathering. The second step consisted in increasing the pH of leachate solution (from 2 to 5) in the presence of DOPA to form the coprecipitates.

Biotite weathering: The steps involved in the dissolution of biotite are detailed in Tamrat et al. (2018). Briefly, 33 g of ground biotite ($< 50 \mu m$) was leached for 29 days in 1 L batches of constant pH 2 HNO_3 solution (solid:liquid ratio 1:30). Dissolved species (leachate solution) were collected by Tangential Flow Filtration (TFF) (Spectrum Labs) with a cutoff size of 10 kD. The final concentrations of the leachate solution (ICP-AES, Horiba Jobin-Yvon "Ultima C", Longjumeau, France) were Fe 937 μM , Si 1006 μM , Al 614 μM , K 883 μM and Mg 1247 μM .

Synthesis of coprecipitates: 1.25, 12.57, 125.68 and 1256.7 mg of DOPA were added to 100 ml of leachate solution at pH 2. This gave initial molar M:C ratios of 2.72, 0.27, 0.027 and 0.0027, ratios that were then rounded up to 3, 0.3, 0.03 and 0.003 for the purpose of naming the samples in the following. 'Molar metal concentration' stands for combined concentrations of the main complexing metals Fe and Al. Coprecipitates were formed by increasing the pH to 5 by adding 0.2M NaOH (Sigma Aldrich) at a constant rate of 70 $\mu L/min$ (Figure A2). When pH 5 was reached, a 1 ml aliquot of sample was collected for TEM-EDX analyses and the remaining solution was ultra-centrifuged at 400,000g for 2 h to separate coprecipitates from the remaining dissolved species. The settled particles (less than 10 mg) were freeze-dried for EXAFS analyses. The nanophase formed without OM is called No C sample. It is identical to the pH 5 sample described in Tamrat et al. (2018) and is used here for the purpose of comparison.

2.3 Characterization of coprecipitates by TEM-EDX: morphology, size, chemical composition and state of crystallinity

The coprecipitates were characterized using a JEOL JEM 2011 Transmission Electron Microscope (TEM) working at 200 kV at CINaM/ Aix-Marseille University, France. The parameters were 50 000X magnification, 20° tilt angle toward the EDX detector, energy range of 40 keV, corrected counting time of 30 s, constant beam density $\sim 63.5 \text{ pA.cm}^{-2}$. Fe, Si, Al, K, and Mg were quantified using the Bruker AXS TEM line mark data semi-quantification procedure (Berthonneau et al., 2014). C was detected in all analyzed particles but C quantification is not reliable using this method (note that the low mass of collected

coprecipitates did not allow us to measure C content using an alternative method). The atomic proportions of analyzed elements thus do not include either C or O in the calculation. EDX chemical analyses were performed on individual particles (30 to 60 per sample). The size of the particles analyzed by EDX was manually measured on micrographs.

2.4 Characterization of coprecipitates at the local scale: EXAFS at the Fe K-edge (acquisition, reference compounds, data treatment)

Extended X-ray absorption fine structure (EXAFS) data were collected at the Fe K-edge (7112 eV) at ESRF synchrotron source on the FAME beam line (Grenoble, France) and at ELETTRA synchrotron, beam line 11.1 (Trieste, Italy). Spectra were collected using Si(220) at the ESRF and Si(111) double crystal monochromators at ELETTRA. Data were collected in ambient conditions in both transmission and fluorescence modes (30-element solid-state Ge detector (Canberra, France)).

All the samples were mixed with boron nitride as a diluting agent and pressed into 5 mm diameter pellets. An average of 3 to 5 individual spectra comprised each spectrum taken 107 eV below and 849 eV above the absorption edge of Fe (7112 eV) at a counting rate of 2-9 seconds up to 14.75 \AA^{-1} . To minimize the risk of beam damage and to obtain representative spectra, each spectrum was collected at different pellet locations. Using $\Delta R = \pi/2k$, the minimum distance resolution was determined to be 0.11 \AA . All radial distances referring to Fourier transform functions (FTF) given in the Results section are uncorrected for phase shift.

Fe speciation in the coprecipitates was assessed by linear combination fitting (LCF) using Athena software (Ravel and Newville, 2005) following the data reduction steps of Michalowicz et al. (1979). LCF is meant to quantitatively reproduce EXAFS spectral features by using the smallest number of reference components. The sensitivity of LCF is within the 10-20% range (O'Day et al., 2004), and no more than three reference components were used. During fitting, all weights were restricted to remain between 0 and 1 without forcing their sum to equal 1 (or 100%). The relative goodness-of-fit between the data and the model is described by the residual factor (R-factor, the lower R, the better the fit). The reference standards (Tables B1, B2 and Figure 3) were selected to represent increasing levels of Fe polymerization with iron citrate, Fe-C colloids, Fe dimers, $\text{SRO}_{\text{Fe,Si}}$ and 2L ferrihydrite. Note that descriptions such as Fe-Fe are short for two Fe octahedra interacting, thus making Fe-O-Fe bonds. The designations Fe-Si, Fe-Al and Fe-C are used hereafter to describe Fe interacting with Si tetrahedron, Al octa/tetrahedron and C based molecules, respectively. 2L Ferrihydrite provides the highest Fe polymerization level of all reference compounds with 2.1 edge interactions and 5 double corner interactions (Maillot et al., 2011; Michel et al., 2007). $\text{SRO}_{\text{Fe,Si}}$ is composed of Fe oligomers synthesized at pH 5 in Si rich solutions (Si/Fe=4). These Fe oligomers are characterized by 2.6 edge-sharing and only a 0.6 double corner Fe-Fe interaction but no Fe-O-Si interactions at pH 5 with this Si/Fe ratio (Doelsch et al., 2000; Doelsch et al., 2001). For Fe dimers, only one edge-sharing coordination has been described (Rose et al., 1996). Fe-C colloids have a minimum 0.4 double and 0.7 single corner Fe-Fe interaction with an additional reference to OM complexing Fe with 1.9 C_1 atoms at 2.82 \AA (monodentate) and 1.5 C_2 atoms at 2.98 \AA (bidentate) (Rose et al., 1998). Iron citrate is the chelation of three carboxylic functional groups of a citrate anion with a central Fe atom producing a tridentate mononuclear complex (IUPAC, 2005). Details of the stages of the linear combination fitting

(LCF) process are given in Table B3 and Figure B1. Modeling of spectra by shell by shell fitting was attempted but did not succeed, probably because of the complexity and heterogeneity of the samples.

3 Results

3.1 TEM-EDX results

TEM micrographs of the coprecipitates are shown in Figure 1. Whatever the M:C ratio, rounded globular particles were formed and aggregated in clusters on the TEM grid. The diameter of the individual spherical particles ranged from 2 to 50 nm for the 'No C', 2 to 40 nm for M:C=3, 5 to 200 nm for M:C=0.3, 10 to 90 nm for M:C=0.03 and 15 to 70 nm for M:C=0.003. In the No C sample, the clusters of rather small particles on the one hand, and clusters of large particles on the other hand are described in Tamrat et al. (2018). In M:C=3 and M:C=0.3, some clusters of smaller particles were also occasionally observed, but in contrast to the No C sample, their occurrence was rare and differentiating smaller and larger particles was more delicate. Regardless of the size of the particles, electron diffraction analyses (Figure 1) revealed a diffused pattern for all the samples. This pattern is characteristic of amorphous structures.

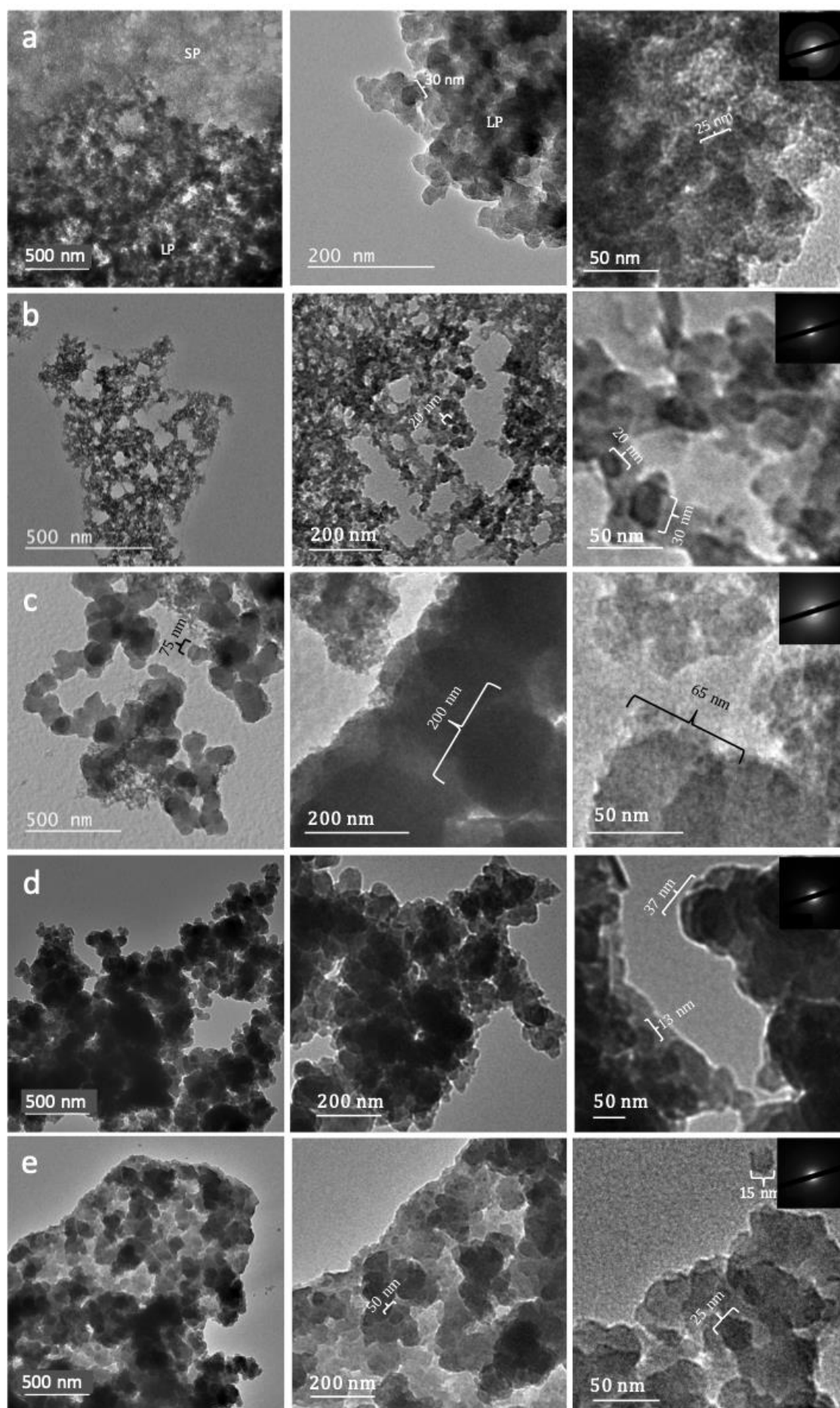


Figure 1: TEM electron micrographs of coprecipitate series at pH=5: (a) 'No C', (b) M:C=3, (c) M:C=0.3, (d) M:C=0.03 and (e) M:C=0.003. Electron diffraction patterns are shown in the upper right of the 50 nm scale pictures. In the No C sample (a), LP stands for areas of larger particles and SP for smaller particles.

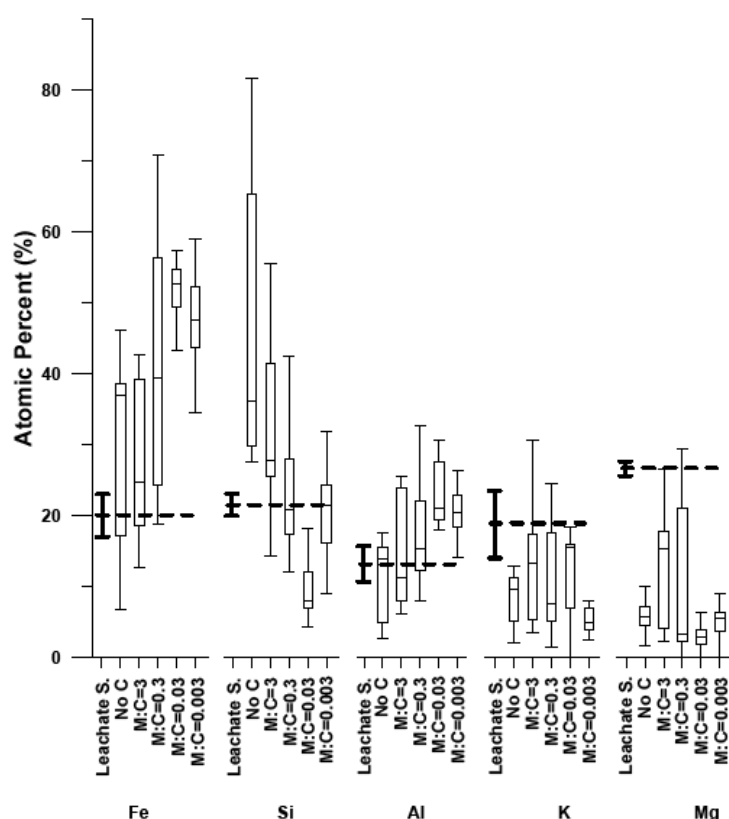


Figure 2: TEM-EDX chemical analysis of nanophases (No C) and coprecipitates at the four M:C ratios expressed in stoichiometric atomic % (excluding C and O). The "box-and-whisker" plots represent median values, the upper and lower quartiles, as well as the min and max of the data. Number of analyzed particles: No C n=33; M:C=3 n= 42; M:C=0.3 n=30; M:C=0.03 n=40; M:C=0.003 n=60. For the purpose of comparison, the chemical composition of the leachate solution (Leachate S.) is also shown as dashed lines with their respective error values.

3.2 Fe atomic range order – EXAFS at the Fe k-edge

3.2.1 Raw data analysis

EXAFS spectra and Fourier transform functions (FTF) are shown in Figure 3. For the reference samples, in transiting from the '2L Ferrihydrite, $\text{SRO}_{\text{Fe,Si}}$ and Fe Dimers' to 'Fe-C Colloids and Iron citrate' standards, the positive oscillations at $\sim 5.2 \text{ \AA}^{-1}$ and $\sim 7.5 \text{ \AA}^{-1}$ on the EXAFS curves, which are characteristic signals of Fe-Fe interactions, lost intensity. Instead, a shoulder

emerged at $\sim 5.7 \text{ \AA}^{-1}$, which is characteristic of Fe-O-C bonds. For the No C sample, in k-space, a low intensity positive oscillation was recorded at $\sim 7.5 \text{ \AA}^{-1}$. The signal at $\sim 5.2 \text{ \AA}^{-1}$ was low intensity and appeared as a shoulder. In R-space, a strong signal of a broad peak with a shoulder was observed in the range 2.4-3.2 \AA due to Fe-Fe octahedra edge and double corner interactions respectively (distances are uncorrected for phase shift and have to be shifted by 0.3-0.4 \AA from crystallographic positions toward long distances) (Bottero et al., 1994; Maillot et al., 2011; Manceau and Gates, 1997; Manceau et al., 2000). M:C=3 showed similar signals appearing in k-space but at reduced intensities. In R-space, the signal around 2.9 \AA narrowed to a single peak in the range 2.55-3.05 \AA (with no shoulder). M:C=0.3, in both k and R-spaces, spectra did not exhibit clear markers of Fe-Fe octahedra interactions, but an R-space peak was detected at $\sim 2.4 \text{ \AA}$, a signal of Fe-C interactions. M:C=0.03 and M:C=0.003 samples showed similar EXAFS signals. In both cases, an EXAFS shoulder was detected at $\sim 5.7 \text{ \AA}^{-1}$ and a second shell R-space peak at $\sim 2.4 \text{ \AA}$. This peak (uncorrected for phase shift) was at a radial distance shorter than the shortest possible Fe-Fe interaction (Rose et al., 1998). The shortest Fe-Fe interaction is related to octahedra face sharing with a Fe-Fe distance of 2.9 \AA as in hematite.

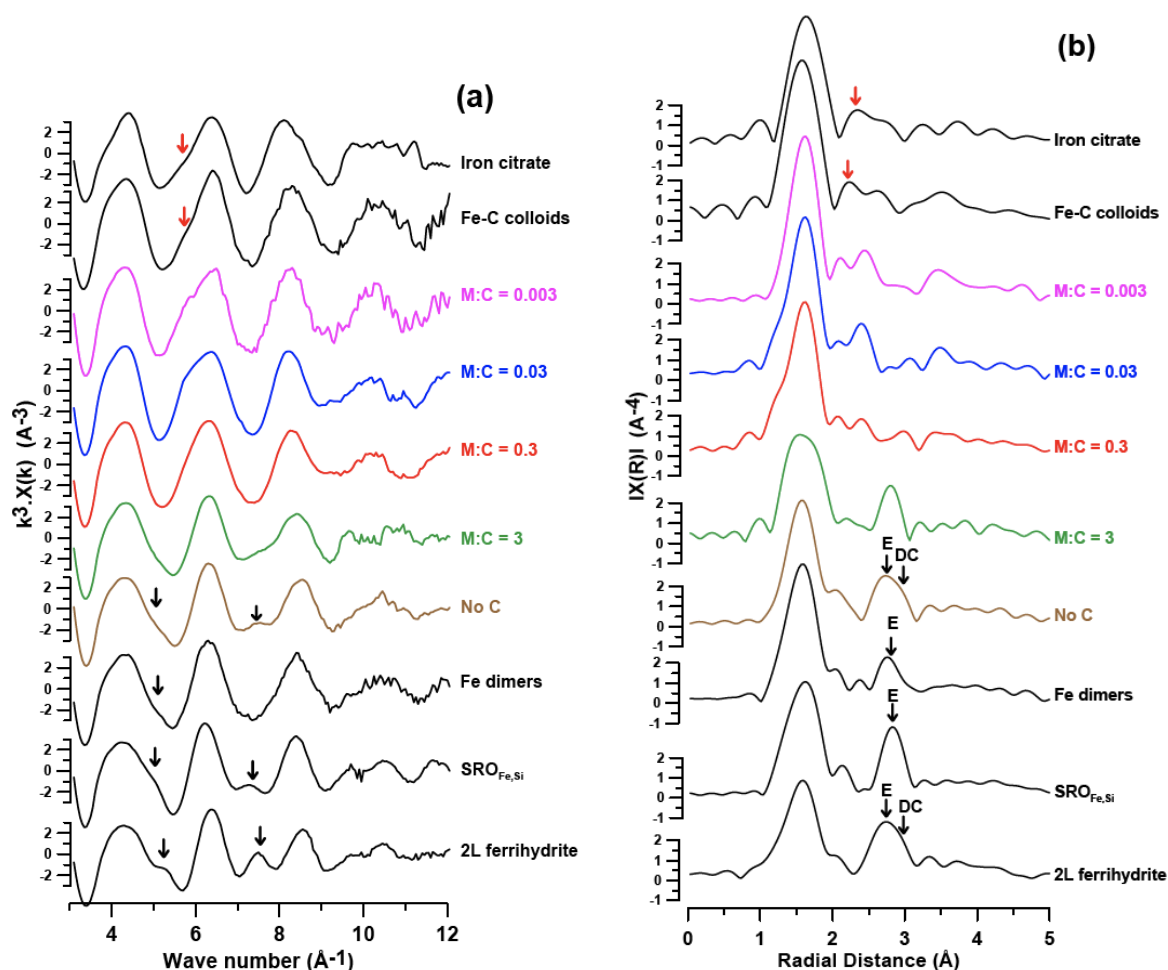


Figure 3: (a) EXAFS/k-space plots and (b) FTF/R-space plots. FTF peaks between 1.2-2 \AA correspond to the first coordination sphere of oxygen atoms. On references, markers of Fe-C interactions (red arrows) occur between ~ 2.2 and $\sim 2.5 \text{ \AA}$ and Fe-Fe octahedra (black arrows) at ~ 2.7 and $\sim 3.0 \text{ \AA}$ (for edge (E) and double corner (DC) interactions respectively). Radial distances are not corrected for phase shift.

3.2.2 Quantitative analysis of EXAFS data using linear combination fitting (LCF)

LCF fits are presented in supplementary information (Figure B1) and summarized in Table 1. The local structure of phases formed with No C were fitted by a combination of 44% of 2L Ferrihydrite, with 33% of Fe Dimers and 25% of $\text{SRO}_{\text{Fe,Si}}$. In the case of M:C=3 samples (compared to No C samples) the collective contribution of purely Fe containing standards decreased from 102% to 82% (2L Ferrihydrite at 37% and $\text{SRO}_{\text{Fe,Si}}$ at 45%). Additionally, significant contributions to the fit were achieved with iron citrate standard at 30%. At a 10-fold increase in C (M:C=0.3), the dominating contributions to fit shifted from Fe-Fe to Fe-C containing reference standards, i.e., the fit from C containing standards (iron citrate + Fe-C colloids) increased from 30% to 72%. And from purely Fe containing standards, contributions to fit decreased from 82% to a sole contribution of 35% from $\text{SRO}_{\text{Fe,Si}}$. A further 10-fold increase in C concentration (M:C=0.03) resulted in a decrease in the Fe-Fe contribution from 35% to 14%, whereas Fe-C contributions (iron citrate and Fe-C colloids) collectively increased from 72% to 94%. With a maximum C content of M:C=0.003, the differences with the M:C 0.03 were not significant and the Fe speciation was considered to be equivalent in the two samples.

Table 1: Proportions of Fe-O-C and Fe-O-Fe bounds estimated by linear combination fitting. Proportions under the three reference standards designated "Fe-O-Fe" show contributions to fit from pure Fe to Fe interactions. Fe-C colloids represent higher Fe to C interaction with a low but significant Fe to Fe interaction. Fe citrate represents pure Fe to C interactions. The error in the proportions was estimated at around 15%. R-factor indicates the relative goodness-of-fit between the data and the model (values close to 0 represent the best fits, see supplementary information for details).

	Iron Citrate	Fe-C Colloids	Fe Dimers	$\text{SRO}_{\text{Fe,Si}}$	2L Ferrihydrite	Sum	R-factor
	Fe-O-C		Fe-O-Fe				
	Fe-O-C	+ Fe-O-Fe					
No C			0.33	0.25	0.44	1.02	0.015
M:C=3	0.30			0.45	0.37	1.12	0.010
M:C=0.3	0.27	0.45		0.35		1.06	0.038
M:C=0.03	0.41	0.53		0.14		1.08	0.059
M:C=0.003	0.59	0.47				1.07	0.055

4 Discussion

4.1 Three types of structures of Fe-Al-Si-coprecipitates as a function of the M:C ratio

The contribution of Si, Fe and Al shown in the ternary diagrams of Figure 4, as well as the speciation of Fe and the size range of particles summarized in Figure 5, highlighted three main types of coprecipitate structures:

- *Type I: high M:C ratio ($M:C=3$)*. Coprecipitates are mainly represented by amorphous spherical Si, Fe, Al particles 2-40 nm in size (Figure 5). When only Fe, Al and Si are considered, Si is the main component (30% to 70%, Figure 4). Fe is only present at 20-50% and Al at 10-30%. The local structure of Fe is dominated by small oligomers of Fe octahedra. This local structure is close to the "No C" nanophase structure described in Tamrat et al. (2018) for samples with a pH of 5 precipitated without OM. Ferrihydrite is not formed in the Type I coprecipitates, likely due to the dominating presence of Si oligomers (Doelsch et al., 2000; Doelsch et al., 2001; Tamrat et al., 2018). However, the presence of Si does not prevent the formation of Fe-O-C binding, since 20% to 30% of the Fe present in the coprecipitates is linked to OM.

- *Type II: intermediate M:C ratio ($M:C=0.3$)*. Coprecipitates are mainly represented by Fe, Si, Al particles 5-200 nm in size, i.e. by far the largest coprecipitates in the present study. In contrast to Type I, Fe is the main component (25-75%) of most of the particles. Si (15-50%) no longer dominates the composition of the coprecipitates but remains present in significant proportions in the structure. Al (10-35%), is anti-correlated with Fe. The local structure of Fe is dominated by bonds with OM (70%) but 30% of Fe remains linked to Fe. Small oligomers of a few Fe octahedra are thus preserved in Type II coprecipitates. Al may also bind OM, but the methods used here were unable to probe Al speciation to confirm it. Thus, the Type II structure, which combines the network of small oligomers of Si, Fe, and Al associated with OM and monomeric Fe-OM, forms the largest coprecipitates.

- *Type III: low M:C ratio ($M:C=0.03$ and $M:C=0.003$)*. Coprecipitates of Type III are mainly represented by Fe, Si, Al particles 10-90 nm in size. Fe is the main component (45-70%), but is slightly depleted compared to Type II Fe content. Conversely, Si (5-40%) and Al (15-35%) are slightly enriched compared to Type II. Fe is almost exclusively bound to C (Figure 5) showing that the monomeric Fe-OM complexation is likely the main interaction in the formation of coprecipitates when large quantities of OM are present. However, a few Fe-Fe dimers, trimers or small oligomers may remain, since LCF showed Fe-Fe interactions for $M:C=0.03$, but within the uncertainty of the method. We hypothesize that within the coprecipitates at M:C lower than 0.03, Al and Si may form small oligomers occluded in the Fe-OM matrix and that Al may also bind OM.

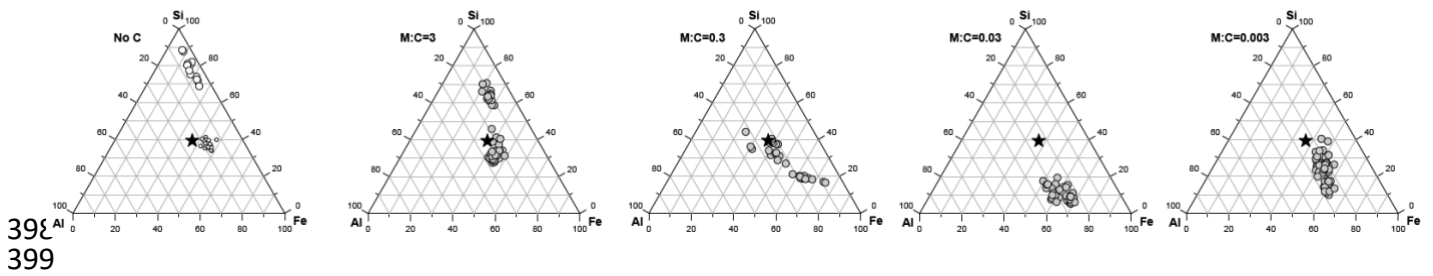


Figure 4: Ternary diagrams of Fe, Si and Al atomic proportions in the analyzed particles. White dots: smaller and larger nanophases in the No C sample (Tamrat et al. 2018). Grey dots: coprecipitates for the four M:C ratios. The black star represents the initial composition of the leachate solution.

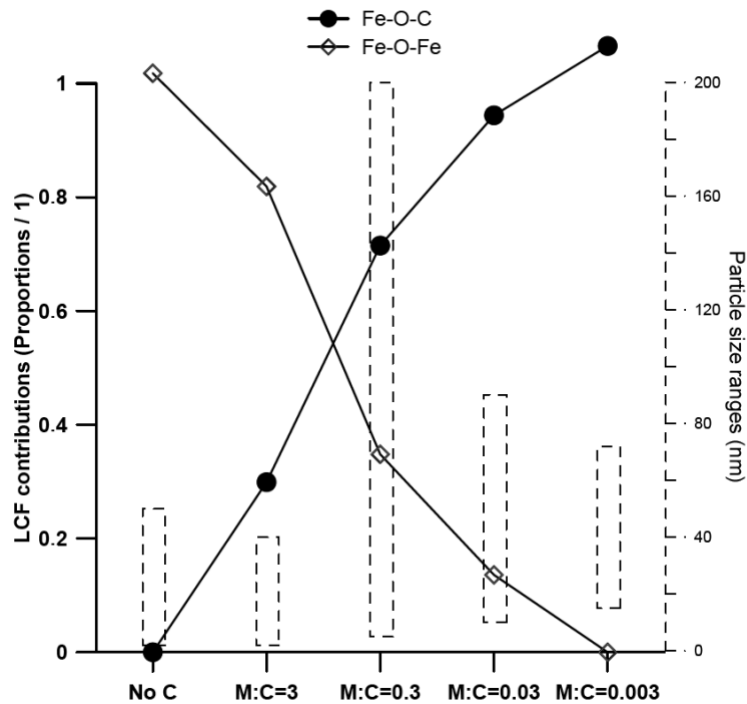


Figure 5: Solid line: LCF contributions of Fe-O-Fe and Fe-O-C interactions. Fe-O-Fe represents contributions from Fe dimers, $\text{SRO}_{\text{Fe,Si}}$ and 2L Ferrihydrite, while Fe-O-C represents contributions from Fe-C colloids and iron citrate reference standards. Dashed bars: particle size ranges.

The mixtures of mononuclear metal-organic complexes and metal hydroxides has already been described in many studies that synthesized Fe-coprecipitates, Al-coprecipitates and Fe-Al-coprecipitates (Karlsson and Persson, 2010, 2012; Mikutta et al., 2010; Mikutta et al., 2014; Nierop et al., 2002). Their proportions also varied as a function of the M:C ratios. For example, Chen et al. (2016) described three types of local structures in Fe-coprecipitates: (1) in low C systems, the ferrihydrite-like Fe domains were precipitated as the core and covered by the OM shells; (2) in systems with intermediate C content, the emerging Fe-C bonding suggested a more substantial association between Fe domains including edge- and corner-sharing Fe octahedra and OM; (3) in systems with high C content, only corner-sharing Fe octahedra along with Fe-C bond were found. In our system, even though the system was too complex to perform shell by shell fitting to model the contributions of edges and corners, as we did for the nanophases of the No C samples (Tamrat et al., 2018), we observed a similar trend for Fe speciation. The level of Fe polymerization decreased with an increase in C content. However, the main difference between this and the pure Fe system was the presence of Si (and to a

lesser extent of Al) that in particular prevents the polymerization of Fe into ferrihydrite domains even at very low OM content. The second significant difference was the presence of Si and Al in the coprecipitates, whatever the M:C ratio.

4.2 Conceptual model of coprecipitate structure in a Fe, Al, Si and OM system

4.2.1 Structure of Type II coprecipitates: “nanoCLICs”

The three types of local structures described above represent three snapshots of an increasing scale of C content in which we multiplied the concentration of OM by 10 at each step. On a linear continuum of the M:C ratio, the local structure of the coprecipitates formed at pH 5 therefore gradually shifted from Type I to Type III with increasing C content. The Type I structure resembles that of nanophases with no OM, and the structure of the nanophases is detailed in Tamrat et al. (2018). At the opposite end of the M:C scale, in the Type III structure, OM stabilization is dominated by monomeric metal-OM interactions. Beyond the fact that Si oligomers are present in small amounts in the coprecipitates, the structure that stabilizes OM is likely close to that of Fe and Al monomeric complexes described in previous papers (Chen et al., 2016; Eusterhues et al., 2008; Karlsson and Persson, 2010, 2012; Karlsson et al., 2008; Mikutta et al., 2010; Schwertmann et al., 2005). Between Type I and III, the range at which Type II is observed is narrow and reduced to M:C between approximately 3 and 0.3. This range could be an important range for C stabilization processes as it corresponds to the largest particles that coprecipitated in our study (Figure 5). This range of M:C ratios also corresponds to the values observed in andosols (Basile-Doelsch et al., 2005; Basile-Doelsch et al., 2007). As Type II has never been described in previous work, we propose a model to represent a Type II structure of the coprecipitates (Figure 6).

The frame of Type II coprecipitates could be formed by a loose and irregular 3D network of amorphous small oligomers of Fe, Si and Al forming an “open” branched mineral skeleton. In this network, the OMs are linked in three different ways: (1) OM binding to Fe (and Al) octahedra that belong to the Al, Si, Fe oligomers network; (2) OM binding to Fe (and Al) monomers, located in the porosity of this network; (3) OM interacting with other OMs by weak bonds (such as Van der Waals or cation bridges (Lutzow et al., 2006)). It is important to note that, in the particular case of DOPA, one molecule may bind simultaneously to two different Fe octahedra (through carboxylate and catecholate bindings). Natural organic compounds may behave in the same way. Together with Van der Waals electrostatic bindings, covalent bindings likely help stabilize the structure of the whole 3D network. We define the Type II structure as “Nanosized Coprecipitates of inorganic oLligomers with organiCs” with the acronym “nanoCLICs”.

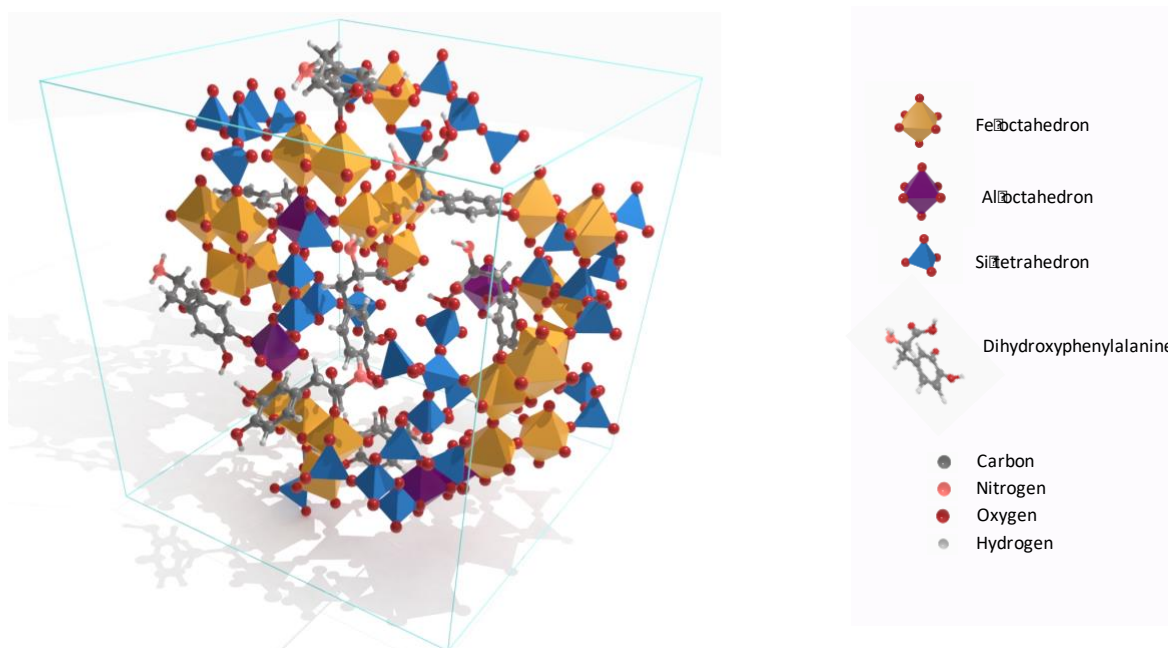


Figure 6 : 3D conceptual model of Nanosized Coprecipitates of inorganic oligomers with organics ("nanoCLICs") in an Fe-Al-Si and DOPA system with initial $0.3 < M:C < 3$. H_2O molecules are not represented to simplify the visualization of the structure. The 3D model can be rotated with Adobe Acrobat using the pdf file provided in the Electronic Annex (a 3D PDF basic function tutorial can be found on <https://www.qwant.com/?q=rotating%20object%20pdf%20adobe%20acrobat&t=videos&o=0:9860450d6f706f26d49065218b7d1c03>).

4.2.2 Comparison with previous models and limits of the model

This model of the structure of nanoCLICs differs from the models proposed in the literature. Previous models of coprecipitates included Fe only as ferrihydrite and monomeric Fe-OM (Eusterhues et al., 2014; Guenet et al., 2017; Kleber et al., 2015). In the model in Figure 6, other major elements potentially present in the soil solution are taken into account. These are mainly Si and Al in the synthetic samples studied here. In the conditions in which we formed the coprecipitates, K and Mg did not significantly contribute to the coprecipitates. However in soils, even if Fe, Si and Al are likely the main contributors, if other elements are present in sufficiently high concentrations and with appropriate physical-chemical conditions, they may also contribute to the structure of nanoCLICs.

Within a network of oligomers on which OM can bind to a very large number of Fe (and Al) octahedra, the model of "core metal hydroxides embedded in an organic matrix" (Chen et al., 2016; Eusterhues et al., 2014; Mikutta et al., 2014) can no longer be applied. Interactions occur at the scale of monomers, dimers, trimers or very small Fe (or Al) oligomers. To represent these interactions, the model thus must be focused at a very local scale. Such a local scale was used by Schulten and Leinweber (2000) to perform molecular simulations. However their model considered large humic molecules and proposed well crystallized Fe oxides as pedogenic oxides. Since the 2000s, these two concepts have been revised (Schmidt et al., 2011), thereby invalidating the results of Schulten and Leinweber's molecular simulations.

A similar local scale was used in the Kleber et al. (2007) conceptual molecular model to illustrate a conceptual view of OM organization at the interfaces with minerals. The model developed by these authors differed significantly from ours in the mineralogical structure of the interface. In their model, the authors considered theoretical mineral surfaces (kaolinite,

Fe oxides) to be flat and well crystallized. But it is likely that such theoretical surfaces only occur exceptionally in soils, mainly because mineral surfaces are subject to alteration (Basile-Doelsch et al., 2015; Churchman and Lowe, 2012). The concept of three superposed OM layers covering the mineral surfaces (Kleber et al., 2007) is likely not strictly applicable to OM interacting with oligomers in nanoCLICs.

It is important to point out that the model presented in Figure 6 also has its limitations. First, it illustrates coprecipitates with a very specific OM, chosen because it can bind to metals in different ways (COOH, phenol, catecholate). These functions are recognized as being particularly conducive to co-precipitation (Mikutta, 2011). The structure of the nanoCLICs could be a little different from that of other molecules of OM: some authors who tested different types of OM observed effects on the density of the coprecipitates for example (Eusterhues et al., 2008; Mikutta et al., 2008). Furthermore, at pHs other than pH 5, the results could also have differed slightly because inorganic oligomers have a different chemistry, with in particular, less Si at pH 4.2 and 7 (Tamrat et al., 2018).

To sum up, the model proposed in Figure 6 provides one example of nanoCLICs with the aim of illustrating the importance of taking at least Fe, Al as well as Si into account in the structure of coprecipitates, even if Si does not bind directly to OM. In a mineral open network with Si in the structure, it is indeed expected that the crystallinity of Fe (and potentially Al) will be lower, implying (1) greater reactivity of Fe (and Al) for OM and (2) a very large specific surface area of inorganic oligomers, forming an open-branched 3D network. These are two key factors in soil OM stabilization (Eusterhues et al., 2014; Jones and Edwards, 1998; Mikutta et al., 2011; Porras et al., 2018; Scheel et al., 2007b), but possibly also in interactions with other charged species in soils.

4.3 Implications for soils

The role of Si in the mechanisms of OM stabilization by SRO have probably been largely underestimated. Unlike Al and Fe, Si does not bind to OM. However, our work showed that its presence limits the polymerization of Fe (and probably of Al) thus increasing the number of Fe (and Al) octahedra available to bind OM. It can thus be expected that, for the same number of Fe (and Al) atoms, a system that also contains Si will be much more reactive toward OM than a system with no Si. The present work suggests that Si could therefore play an important role in the quantities of OM stabilized by nanoCLICs in a soil profile. Future works should focus on that hypothesis.

On the other hand, Si could also play a major role in the persistent reactivity of inorganic oligomers. As proposed by Jones et al. (2009), the presence of Si may limit the progressive aging of the Fe (and Al) phases towards better crystallized and more stable Fe (and Al) oxides. As crystallized Fe oxides are less reactive to OM stabilization than Fe-oligomers (Basile-Doelsch et al., 2007; Basile-Doelsch et al., 2009), the presence of Si would insure the preservation of the very poorly polymerized state and maintain the high specific surface area and high reactivity. Thus, the presence of Si in the structures of the coprecipitates may control not only the amount of OM stabilized by the nanoCLICs, but also the persistence of this OM stabilization potential in the longer term.

The formation of nanoCLICs containing Fe, Si and Al is very likely to occur in most soils, as silicates are the main minerals in the Earth's crust. The "pure" Fe and Al coprecipitates, as studied in synthetic systems, have made it possible to highlight different levels of Fe polymerization (Chen et al., 2016; Eusterhues et al., 2008; Karlsson and Persson, 2010, 2012; Karlsson et al., 2008; Mikutta, 2011; Mikutta et al., 2010; Nierop et al., 2002; Scheel et al., 2007a; Schneider et al., 2010; Schwertmann et al., 2005), but may not be representative of the majority of nanoCLICs in most soils. The occurrence of pure Fe-coprecipitates and Al-coprecipitates is probably limited to very specific environments. In the case of Fe, for example, Fe-coprecipitates may form in environments subjected to redox oscillations (Coward et al., 2018). But in most soils, nanoCLICs likely incorporate a large number of major cations other than Fe and Al, such as Si, Mn (Stuckey et al., 2018), or to a lesser extent more soluble species such as Ca (Rasmussen et al., 2018), Mg or even monovalent species as K (Grand and Lavkulich, 2015), depending on the physical-chemical conditions (concentrations, pH, redox, etc.). Recent studies showed in particular the important role played by Ca in ternary complexation mechanisms (Rowley et al., 2018; Sowers et al., 2018) and its importance in stabilizing OM in rather arid soils and in soils with a pH above 7 (Kramer and Chadwick, 2018; Rasmussen et al., 2018).

Within a soil profile, nanoCLICs could also be characterized by high variability in space, over time and in their structure. It is very likely that in a given soil profile, amorphous Fe Si Al nanophase (Type I), nanoCLICs (type II) and monomeric Fe complex (type III) will be found simultaneously at different microsites. Physical-chemical conditions at a microsite can also vary over time, which may lead to time-dependent variations in the structure of nanoCLICs. At some microsites, as proposed by Keiluweit et al. (2015) in the rhizosphere, the de-structuration of SRO-OM may also occur upon biologic stimulation. The dynamics of nanoCLICs structures should thus also be considered in future studies of OM stabilization.

5 Conclusion

Organo-mineral interactions are recognized as key factors in stabilizing organic matter (OM) in soils, and short-range order minerals (SRO) are increasingly considered as key mineral nanophases in the control of soil OM dynamics. In the present work, we have shown that:

- Fe-coprecipitate and Al-coprecipitate systems are likely not the only coprecipitates to consider in SRO-OM stabilization issues, because they do not fit the complex chemical composition of soil solutions that occur in soils;
- In soils in which silicate minerals are present and provide a range of cations upon weathering ($\text{Fe}(\text{OH})^{2+}$, $\text{Al}(\text{OH})^{2+}$, $\text{Si}(\text{OH})_4$, Mg^{2+} , Ca^{2+} , K^{2+} etc.), at least Si may be an important component in the mineral structure of the coprecipitates, whatever the concentration of C;
- In the case of intermediate C contents, we propose a structural model of coprecipitates in which amorphous small oligomers of Fe (~70%), Si (~20%), Al (~10%) form an amorphous, open-branched 3D network. In this mineral skeleton, organic compounds are linked either by bonds with Fe and Al to the network, by monomeric Fe-O-C in the porosity of the network, or by weak bonds with OM. We propose to name the structure "Nanosized Coprecipitates of inorganic oLligomers with organiCs" with the acronym "nanoCLICs".
- In nanoCLICs, Si does not bind directly with OM. However, it prevents the polymerization of Fe and Al phases into crystalline structures, thereby insuring large

582 amounts of Fe and Al are available to bind with OM and hence for C stabilization. The
583 presence of Si may also limit the progressive aging of the Fe and Al phases into better
584 crystallized oxides, thus insuring the preservation of the very poorly crystallized state
585 and maintaining the high C stabilization potential of inorganic oligomers.
586
587

6 Acknowledgements

We would like to thank the European Synchrotron Radiation Facility (ESRF) (Grenoble, France) and ELETTRA synchrotron (Trieste, Italy) and their respective teams at the FAME and 11.1 beam lines for their kind and expert assistance during the EXAFS measurements. We also thank Patrice Thaunay (CIRAD) who designed the nanoCLICs 3D illustration.

7 Funding:

This work was supported by Aix-Marseille University doctoral school ED251, ANR (NanoSoilC ANR-16-CE01-0012-02 project) and the *Institut Universitaire de France*.

8 References

- Angelico, R., Ceglie, A., He, J.Z., Liu, Y.R., Palumbo, G. and Colombo, C. (2014) Particle size, charge and colloidal stability of humic acids coprecipitated with Ferrihydrite. *Chemosphere* 99, 239-247.
- Baldock, J.A. and Skjemstad, J.O. (2000) Role of the soil matrix in protecting natural organic materials against biological attack. *Organic Chemistry* 31.
- Basile-Doelsch, I., Amundson, R., Stone, W., Masiello, C., Bottero, J., Colin, F., Masin, F., Borschneck, D. and Meunier, J.D. (2005) Mineral control of soil organic carbon dynamic in an allophanic soil (La Réunion). *Eur. J. Soil Sci.* 56, 689-703.
- Basile-Doelsch, I., Amundson, R., Stone, W.E.E., Borschneck, D., Bottero, J.Y., Moustier, S., Masin, F. and Colin, F. (2007) Mineral control of carbon pools in a volcanic soil horizon. *Geoderma* 137, 477-489.
- Basile-Doelsch, I., Balesdent, J. and Rose, J. (2015) Are Interactions between Organic Compounds and Nanoscale Weathering Minerals the Key Drivers of Carbon Storage in Soils? *Environ. Sci. Technol.* 49, 3997-3998.
- Basile-Doelsch, I., Brun, T., Borschneck, D., Masion, A., Marol, C. and Balesdent, J. (2009) Effect of landuse on organic matter stabilized in organomineral complexes: A study combining density fractionation, mineralogy and $\delta^{13}\text{C}$. *Geoderma* 151, 77-86.
- Berthonneau, J., Grauby, O., Ferrage, E., Vallet, J.-M., Bromblet, P., Dessandier, D., Chaudanson, D. and Baronnet, A. (2014) Impact of swelling clays on the spalling decay of building limestones: insights from X-ray diffraction profile modeling. *European Journal of Mineralogy* 26, 643-656.
- Bonnard, P., Basile-Doelsch, I., Balesdent, J., Masion, A., Borschneck, D. and Arrouays, D. (2012) Organic matter content and features related to associated mineral fractions in an acid, loamy soil. *Eur. J. Soil Sci.* 63, 625-636.
- Bottero, J.Y., Manceau, A., Villieras, F. and Tchoubar, D. (1994) Structure and mechanisms of formation of $\text{FeOOH}(\text{Cl})$ polymers *Langmuir* 10, 316–319.
- Chen, C.M., Dynes, J.J., Wang, J. and Sparks, D.L. (2014) Properties of Fe-Organic Matter Associations via Coprecipitation versus Adsorption. *Environ. Sci. Technol.* 48, 13751-13759.

626 Chen, K.-Y., Chen, T.-Y., Chan, Y.-T., Cheng, C.-Y., Tzou, Y.-M., Liu, Y.-T. and Teah, H.-Y. (2016)
 627 Stabilization of Natural Organic Matter by Short-Range-Order Iron Hydroxides. *Environ. Sci.*
 628 *Technol.* 50, 12612-12620.

629 Churchman, G.J. and Lowe, D.J. (2012) Alteration, formation, and occurrence of minerals in
 630 soils, in: Huang, P.M., Li, Y., Sumner, M.E. (Eds.), *Handbook of soil sciences*. CRC Press (Taylor
 631 & Francis), Boca Raton, FL, pp. 20.21-20.72.

632 Coward, E.K., Thompson, A. and Plante, A.F. (2018) Contrasting Fe speciation in two humid
 633 forest soils: Insight into organomineral associations in redox-active environments.
 634 *Geochimica Et Cosmochimica Acta* 238, 68-84.

635 Doelsch, E., Rose, J., Masion, A., Bottero, J.Y., Nahon, D. and Bertsch, P.M. (2000) Speciation
 636 and crystal chemistry of iron(III) chloride hydrolyzed in the presence of SiO₄ ligands. 1. An
 637 FeK-edge EXAFS study. *Langmuir* 16, 4726-4731.

638 Doelsch, E., Rose, J., Masion, A., Bottero, J.Y., Nahon, D. and Bertsch, P.M. (2002) Hydrolysis
 639 of iron(II) chloride under anoxic conditions and influence of SiO₄ ligands. *Langmuir* 18, 4292-
 640 4299.

641 Doelsch, E., Stone, W.E.E., Petit, S., Masion, A., Rose, J., Bottero, J.-Y. and Nahon, D. (2001)
 642 Speciation and crystal chemistry of Fe(III) chloride hydrolyzed in the presence of SiO₄
 643 ligands. 2. Characterization of Si-Fe aggregates by FTIR and ²⁹Si solid-state NMR. *Langmuir*
 644 17, 1399-1405.

645 Du, H., Peacock, C.L., Chen, W. and Huang, Q. (2018) Binding of Cd by ferrihydrite organo-
 646 mineral composites: Implications for Cd mobility and fate in natural and contaminated
 647 environments. *Chemosphere* 207, 404-412.

648 Eusterhues, K., Neidhardt, J., Hadrich, A., Kusel, K. and Totsche, K.U. (2014) Biodegradation
 649 of ferrihydrite-associated organic matter. *Biogeochemistry* 119, 45-50.

650 Eusterhues, K., Rennert, T., Knicker, H., Kogel-Knabner, I., Totsche, K.U. and Schwertmann,
 651 U. (2011) Fractionation of Organic Matter Due to Reaction with Ferrihydrite: Coprecipitation
 652 versus Adsorption. *Environ. Sci. Technol.* 45, 527-533.

653 Eusterhues, K., Wagner, F.E., Hausler, W., Hanzlik, M., Knicker, H., Totsche, K.U., Kogel-
 654 Knabner, I. and Schwertmann, U. (2008) Characterization of Ferrihydrite-Soil Organic Matter
 655 Coprecipitates by X-ray Diffraction and Mossbauer Spectroscopy. *Environ. Sci. Technol.* 42,
 656 7891-7897.

657 Finley, B.K., Dijkstra, P., Rasmussen, C., Schwartz, E., Mau, R.L., Liu, X.-J.A., van Gestel, N. and
 658 Hungate, B.A. (2018) Soil mineral assemblage and substrate quality effects on microbial
 659 priming. *Geoderma* 322, 38-47.

660 Grand, S. and Lavkulich, L.M. (2015) Short-range order mineral phases control the
 661 distribution of important macronutrients in coarse-textured forest soils of coastal British
 662 Columbia, Canada. *Plant and Soil* 390, 77-93.

663 Guenet, H., Davranche, M., Vantelon, D., Gigault, J., Prevost, S., Tache, O., Jaksch, S., Pedrot,
 664 M., Dorcet, V., Boutier, A. and Jestin, J. (2017) Characterization of iron-organic matter nano-
 665 aggregate networks through a combination of SAXS/SANS and XAS analyses: impact on As
 666 binding. *Environmental Science-Nano* 4, 938-954.

667 IUPAC (2005) *Nomenclature of Inorganic Chemistry*. The Royal Society of Chemistry.

668 Jones, A.M., Collins, R.N., Rose, J. and Waite, T.D. (2009) The effect of silica and natural
669 organic matter on the Fe(II)-catalysed transformation and reactivity of Fe(III) minerals.
670 *Geochimica et Cosmochimica Acta* 73, 4409-4422.

671 Jones, D.L. and Edwards, A.C. (1998) Influence of sorption on the biological utilization of two
672 simple carbon substrates. *Soil Biol. Biochem.* 30, 1895-1902.

673 Karlsson, T. and Persson, P. (2010) Coordination chemistry and hydrolysis of Fe(III) in a peat
674 humic acid studied by X-ray absorption spectroscopy. *Geochimica Et Cosmochimica Acta* 74,
675 30-40.

676 Karlsson, T. and Persson, P. (2012) Complexes with aquatic organic matter suppress
677 hydrolysis and precipitation of Fe(III). *Chemical Geology* 322, 19-27.

678 Karlsson, T., Persson, P., Skyllberg, U., Mörtz, C.-M. and Giesler, R. (2008) Characterization of
679 Iron(III) in Organic Soils Using Extended X-ray Absorption Fine Structure Spectroscopy.
680 *Environ. Sci. Technol.* 42, 5449-5454.

681 Keiluweit, M., Bougoure, J.J., Nico, P.S., Pett-Ridge, J., Weber, P.K. and Kleber, M. (2015)
682 Mineral protection of soil carbon counteracted by root exudates. *Nature Clim. Change* 5,
683 588-595.

684 Kleber, M., Eusterhues, K., Keiluweit, M., Mikutta, C., Mikutta, R. and Nico, P.S. (2015)
685 Chapter One - Mineral–Organic Associations: Formation, Properties, and Relevance in Soil
686 Environments, in: Donald, L.S. (Ed.), *Advances in Agronomy*. Academic Press, pp. 1-140.

687 Kleber, M., Sollins, P. and Sutton, R. (2007) A conceptual model of organo-mineral
688 interactions in soils: self-assembly of organic molecular fragments into zonal structures on
689 mineral surfaces. *Biogeochemistry* 85, 9-24.

690 Kögel-Knabner, I., Guggenberger, G., Kleber, M., Kandeler, E., Kalbitz, K., Scheu, S.,
691 Eusterhues, K. and Leinweber, P. (2008) Organo-mineral associations in temperate soils:
692 Integrating biology, mineralogy, and organic matter chemistry. *Journal of Plant Nutrition and*
693 *Soil Science* 171, 61-82.

694 Kramer, M.G. and Chadwick, O.A. (2018) Climate-driven thresholds in reactive mineral
695 retention of soil carbon at the global scale. *Nature Climate Change* 8, 1104-1108.

696 Lehmann, J. and Kleber, M. (2015) The contentious nature of soil organic matter. *Nature*
697 528, 60-68.

698 Levard, C., Doelsch, E., Basile-Doelsch, I., Abidin, Z., Miche, H., Masion, A., Rose, J.,
699 Borschneck, D. and Bottero, J.Y. (2012) Structure and distribution of allophanes, imogolite
700 and proto-imogolite in volcanic soils. *Geoderma* 183–184, 100-108.

701 Lutzow, M.v., Kögel-Knabner, I., Ekschmitt, K., Matzner, E., Guggenberger, G., Marschner, B.
702 and Flessa, H. (2006) Stabilization of organic matter in temperate soils: mechanisms and
703 their relevance under different soil conditions - a review. *Eur. J. Soil Sci.* 57, 426-445.

704 Maillot, F., Morin, G., Wang, Y.H., Bonnin, D., Ildefonse, P., Chaneac, C. and Calas, G. (2011)
705 New insight into the structure of nanocrystalline ferrihydrite: EXAFS evidence for
706 tetrahedrally coordinated iron(III). *Geochimica Et Cosmochimica Acta* 75, 2708-2720.

707 Manceau, A. and Gates, W.P. (1997) Surface Structural Model for Ferrihydrite. *Clays and Clay*
708 *Minerals* 45, 448-460.

709 Manceau, A., Schlegel, M.L., Musso, M., Sole, V.A., Gauthier, C., Petit, P.E. and Trolard, F.
 710 (2000) Crystal chemistry of trace elements in natural and synthetic goethite. *Geochim.*
 711 *Cosmochim. Acta* 64, 3643–3661.

712 Masion, A. and Bertsch, P.M. (1997) Aluminium speciation in the presence of wheat root cell
 713 walls: A wet chemical study. *Plant Cell and Environment* 20, 504-512.

714 Masion, A., Vilg -Ritter, A., Rose, J., Stone, W.E.E., Teppen, B.J., Rybacki, D. and Bottero, J.Y.
 715 (2000) Coagulation-flocculation of natural organic matter with Al salts: speciation and
 716 structure of the aggregates. *Environ. Sci. Technol.* 34, 3242-3246.

717 Michalowicz, A., Girerd, J. and Goulon, J. (1979) Exafs Determination of the Copper Oxalate
 718 Structure - Relation Between Structure and Magnetic-Properties. *Inorg. Chem.* 18, 3004–
 719 3010.

720 Michel, F.M., Ehm, L., Antao, S.M., Lee, P.L., Chupas, P.J., Liu, G., Strongin, D.R., Schoonen,
 721 M.A.A., Phillips, B.L. and Parise, J.B. (2007) The Structure of Ferrihydrite, a Nanocrystalline
 722 Material. *Science* 316, 1726-1729.

723 Mikutta, C. (2011) X-ray absorption spectroscopy study on the effect of hydroxybenzoic acids
 724 on the formation and structure of ferrihydrite. *Geochimica et Cosmochimica Acta* 75, 5122-
 725 5139.

726 Mikutta, C., Frommer, J., Voegelin, A., Kaegi, R. and Kretzschmar, R. (2010) Effect of citrate
 727 on the local Fe coordination in ferrihydrite, arsenate binding, and ternary arsenate complex
 728 formation. *Geochimica et Cosmochimica Acta* 74, 5574-5592.

729 Mikutta, C., Mikutta, R., Bonneville, S., Wagner, F., Voegelin, A., Christl, I. and Kretzschmar,
 730 R. (2008) Synthetic coprecipitates of exopolysaccharides and ferrihydrite. Part I:
 731 Characterization. *Geochimica et Cosmochimica Acta* 72, 1111-1127.

732 Mikutta, R., Lorenz, D., Guggenberger, G., Haumaier, L. and Freund, A. (2014) Properties and
 733 reactivity of Fe-organic matter associations formed by coprecipitation versus adsorption:
 734 Clues from arsenate batch adsorption. *Geochimica Et Cosmochimica Acta* 144, 258-276.

735 Mikutta, R., Mikutta, C., Kalbitz, K., Scheel, T., Kaiser, K. and Jahn, R. (2007) Biodegradation
 736 of forest floor organic matter bound to minerals via different binding mechanisms.
 737 *Geochimica et Cosmochimica Acta* 71, 2569-2590.

738 Mikutta, R., Zang, U., Chorover, J., Haumaier, L. and Kalbitz, K. (2011) Stabilization of
 739 extracellular polymeric substances (*Bacillus subtilis*) by adsorption to and coprecipitation
 740 with Al forms. *Geochimica et Cosmochimica Acta* 75, 3135-3154.

741 Minasny, B., Malone, B.P., McBratney, A.B., Angers, D.A., Arrouays, D., Chambers, A.,
 742 Chaplot, V., Chen, Z.S., Cheng, K., Das, B.S., Field, D.J., Gimona, A., Hedley, C.B., Hong, S.Y.,
 743 Mandal, B., Marchant, B.P., Martin, M., McConkey, B.G., Mulder, V.L., O'Rourke, S., Richer-
 744 de-Forges, A.C., Odeh, I., Padarian, J., Paustian, K., Pan, G.X., Poggio, L., Savin, I., Stolbovoy,
 745 V., Stockmann, U., Sulaeman, Y., Tsui, C.C., Vagen, T.G., van Wesemael, B. and Winowiecki, L.
 746 (2017) Soil carbon 4 per mille. *Geoderma* 292, 59-86.

747 Nierop, K.G.J., Jansen, B. and Verstraten, J.A. (2002) Dissolved organic matter, aluminium
 748 and iron interactions: precipitation induced by metal/carbon ratio, pH and competition.
 749 *Science of the Total Environment* 300, 201-211.

750 O'Day, P.A., Rivera, N., Root, R. and Carroll, S.A. (2004) X-ray absorption spectroscopic study
 751 of Fe reference compounds for the analysis of natural sediments. *American Mineralogist* 89,
 752 572-585.

753 Paustian, K., Lehmann, J., Ogle, S., Reay, D., Robertson, G.P. and Smith, P. (2016) Climate-
 754 smart soils. *Nature* 532, 49-57.

755 Pokrovski, G.S. and Schott, J. (1998) Experimental study of the complexation of silicon and
 756 germanium with aqueous organic species: Implications for germanium and silicon transport
 757 and Ge/Si ratio in natural waters. *Geochimica Et Cosmochimica Acta* 62, 3413-3428.

758 Porras, R.C., Hicks Pries, C.E., Torn, M.S. and Nico, P.S. (2018) Synthetic iron (hydr)oxide-
 759 glucose associations in subsurface soil: Effects on decomposability of mineral associated
 760 carbon. *Science of The Total Environment* 613-614, 342-351.

761 Rasmussen, C., Heckman, K., Wieder, W.R., Keiluweit, M., Lawrence, C.R., Berhe, A.A.,
 762 Blankinship, J.C., Crow, S.E., Druhan, J.L., Pries, C.E.H., Marin-Spiotta, E., Plante, A.F.,
 763 Schadel, C., Schimel, J.P., Sierra, C.A., Thompson, A. and Wagai, R. (2018) Beyond clay:
 764 towards an improved set of variables for predicting soil organic matter content.
 765 *Biogeochemistry* 137, 297-306.

766 Ravel, B. and Newville, M. (2005) ATHENA, ARTEMIS, HEPHAESTUS: data analysis for X-ray
 767 absorption spectroscopy using IFEFFIT. *Journal of Synchrotron Radiation* 12, 537-541.

768 Rose, J., Manceau, A., Bottero, J.Y., Masion, A. and Garcia, F. (1996) Nucleation and growth
 769 mechanisms of Fe oxyhydroxide in the presence of PO₄ ions .1. Fe K-edge EXAFS study.
 770 *Langmuir* 12, 6701-6707.

771 Rose, J., Vilge, A., Olivie-Lauquet, G., Masion, A., Frechou, C. and Bottero, J.-Y. (1998) Iron
 772 speciation in natural organic matter colloids. *Colloids and Surfaces A: Physicochemical and*
 773 *Engineering Aspects* 136, 11-19.

774 Rowley, M.C., Grand, S. and Verrecchia, É.P. (2018) Calcium-mediated stabilisation of soil
 775 organic carbon. *Biogeochemistry* 137, 27-49.

776 Saidy, A.R., Smernik, R.J., Baldock, J.A., Kaiser, K. and Sanderman, J. (2015) Microbial
 777 degradation of organic carbon sorbed to phyllosilicate clays with and without hydrous iron
 778 oxide coating. *Eur. J. Soil Sci.* 66, 83-94.

779 Scheel, T., Dorfler, C. and Kalbitz, K. (2007a) Precipitation of dissolved organic matter by
 780 aluminum stabilizes carbon in acidic forest soils. *Soil Science Society of America Journal* 71,
 781 64-74.

782 Scheel, T., Dörfler, C. and Kalbitz, K. (2007b) Precipitation of Dissolved Organic Matter by
 783 Aluminum Stabilizes Carbon in Acidic Forest Soils Abbreviations: DOC, dissolved organic
 784 carbon; DOM, dissolved organic matter; OM, organic matter; UV, ultraviolet. *Soil Science*
 785 *Society of America Journal* 71, 64-74.

786 Schmidt, M.W.I., Torn, M.S., Abiven, S., Dittmar, T., Guggenberger, G., Janssens, I.A., Kleber,
 787 M., Kogel-Knabner, I., Lehmann, J., Manning, D.A.C., Nannipieri, P., Rasse, D.P., Weiner, S.
 788 and Trumbore, S.E. (2011) Persistence of soil organic matter as an ecosystem property.
 789 *Nature* 478, 49-56.

790 Schneider, M.P.W., Scheel, T., Mikutta, R., van Hees, P., Kaiser, K. and Kalbitz, K. (2010)
 791 Sorptive stabilization of organic matter by amorphous Al hydroxide. *Geochimica Et*
 792 *Cosmochimica Acta* 74, 1606-1619.

793 Schulten, H.R. and Leinweber, P. (2000) New insights into organic-mineral particles :
 794 composition, properties, and models of molecular structure. *Biol Fertil Soils* 30, 399-432.

795 Schwertmann, U., Wagner, F. and Knicker, H. (2005) Ferrihydrite-humic associations:
 796 Magnetic hyperfine interactions. *Soil Science Society of America Journal* 69, 1009-1015.

797 Sowers, T.D., Adhikari, D., Wang, J., Yang, Y. and Sparks, D.L. (2018) Spatial Associations and
 798 Chemical Composition of Organic Carbon Sequestered in Fe, Ca, and Organic Carbon Ternary
 799 Systems. *Environ. Sci. Technol.* 52, 6936-6944.

800 Stuckey, J.W., Goodwin, C., Wang, J., Kaplan, L.A., Vidal-Esquivel, P., Beebe, T.P. and Sparks,
 801 D.L. (2018) Impacts of hydrous manganese oxide on the retention and lability of dissolved
 802 organic matter. *Geochemical Transactions* 19, 6.

803 Sutton, R. and Sposito, G. (2005) Molecular Structure in Soil Humic Substances: The New
 804 View. *Environ. Sci. Technol.* 39, 9009-9015.

805 Tamrat, W.Z., Rose, J., Grauby, O., Doelsch, E., Levard, C., Chaurand, P. and Basile-Doelsch, I.
 806 (2018) Composition and molecular scale structure of nanophases formed by precipitation of
 807 biotite weathering products. *Geochimica et Cosmochimica Acta* 229, 53-64.

808 Vilgé, A., Masion, A., Boulangé, T., Rybacki, D. and Bottero, J.Y. (1999a) removal of NOM by
 809 coagulation-flocculation. A pyrolysis GC-MS study. *Environmental Science and Technology* 33,
 810 3027-3032.

811 Vilgé, A., Rose, J., Masion, A. and Bottero, J.Y. (1999b) Chemistry and structure of aggregates
 812 formes with Fe salts and natural organic matter. *Colloids and Surface A : Physicochem. Eng*
 813 *Aspects*, 297-308.

814 Zimmerman, A.R., Chorover, J., Goyne, K.W. and Brantley, S.L. (2004) Protection of
 815 Mesopore-Adsorbed Organic Matter from Enzymatic Degradation. *Environ. Sci. Technol.* 38,
 816 4542-4548.

817

818

FIGURE CAPTIONS

Table 1: Proportions of Fe-O-C and Fe-O-Fe bounds estimated by linear combination fitting. Proportions under the three reference standards designated “Fe-O-Fe” show contributions to fit from pure Fe to Fe interactions. Fe-C colloids represent higher Fe to C interaction with a low but significant Fe to Fe interaction. Fe citrate represents pure Fe to C interactions. The error in the proportions was estimated at around 15%. R-factor indicates the relative goodness-of-fit between the data and the model (values close to 0 represent the best fits, see supplementary information for details).

Figure 1: TEM electron micrographs of coprecipitate series at pH=5: (a) ‘No C’, (b) M:C=3, (c) M:C=0.3, (d) M:C=0.03 and (e) M:C=0.003. Electron diffraction patterns are shown in the upper right of the 50 nm scale pictures. In the No C sample (a), LP stands for areas of larger particles and SP for smaller particles.

Figure 2: TEM-EDX chemical analysis of nanophases (No C) and coprecipitates at the four M:C ratios expressed in stoichiometric atomic % (excluding C and O). The “box-and-whisker” plots represent median values, the upper and lower quartiles, as well as the min and max of the data. Number of analyzed particles: No C n=33; M:C=3 n= 42; M:C=0.3 n=30; M:C=0.03 n=40; M:C=0.003 n=60. For the purpose of comparison, the chemical composition of the leachate solution (Leachate S.) is also shown as dashed lines with their respective error values.

Figure 3: (a) EXAFS/k-space plots and (b) FTF/R-space plots. FTF peaks between 1.2-2Å correspond to the first coordination sphere of oxygen atoms. On references, markers of Fe-C interactions (red arrows) occur between ~2.2 and ~2.5 Å and Fe-Fe octahedra (black arrows) at ~2.7 and ~3.0 Å (for edge (E) and double corner (DC) interactions respectively). Radial distances are not corrected for phase shift.

Figure 4: Ternary diagrams of Fe, Si and Al atomic proportions in the analyzed particles. White dots: smaller and larger nanophases in the No C sample (Tamrat et al. 2018). Grey dots: coprecipitates for the four M:C ratios. The black star represents the initial composition of the leachate solution.

Figure 5: Solid line: LCF contributions of Fe-O-Fe and Fe-O-C interactions. Fe-O-Fe represents contributions from Fe dimers, SRO_{Fe,Si} and 2L Ferrihydrite, while Fe-O-C represents contributions from Fe-C colloids and iron citrate reference standards. Dashed bars: particle size ranges.

Figure 6 : 3D conceptual model of Nanosized Coprecipitates of inorganic oLIgomers with organiCs (“nanoCLICs”) in an Fe Al Si and DOPA system with initial 0.3 <M:C <3. H₂O molecules are not represented to simplify the visualization of the structure. The 3D model can be rotated with Adobe Acrobat using the pdf file provided in the Electronic Annex (a 3D PDF basic function tutorial can be found on <https://www.qwant.com/?q=rotating%20object%20pdf%20adobe%20acrobat&t=videos&o=0:9860450d6f706f26d49065218b7d1c03>).